FULL PAPER

Dalton
www.rsc.org/dalton

Phenolate and phenoxyl radical complexes of Co(II) and Co(III)†

Laurent Benisvy,*[a] Eckhard Bill,[b] Alexander J. Blake,[a] David Collison,[c] E. Stephen Davies,[a] C. David Garner,*[a] Christina I. Guindy,[a] Eric J. L. McInnes,[c] Graeme McArdle,[a] Jonathan McMaster,*[a] Claire Wilson[a] and Joanna Wolowska[c]

[a] *School of Chemistry, The University of Nottingham, University Park, Nottingham, UK NG7 2RD. E-mail: Dave.Garner@nottingham.ac.uk*

[b] *Max-Planck-Instut für Bioanorganische Chemie, Stiftstrasse 34-46, Mülheim an der Ruhr, D-45470, Germany*

[c] *Department of Chemistry, The University of Manchester, Oxford Road, Manchester, UK M13 9PL*

Received 19th July 2004, Accepted 14th September 2004
First published as an Advance Article on the web 4th October 2004

The new phenol–imidazole pro-ligands ^{R}LH react with $Co(BF_4)_2\cdot 6H_2O$ in the presence of Et_3N to form the corresponding $[Co^{II}(^{R}L)_2]$ compound (R = Ph (**1**), PhOMe (**2**), or Bz (**3**)). Also, ^{Bz}LH, reacts with Co(II) in the presence of Et_3N and H_2O_2 to form $[Co^{III}(^{Bz}L)_3]$ (**4**). The structures of **1**·2.5MeCN, **2**·2DMF, **3**·4MeOH, and **4**·4DMF have been determined by X-ray crystallography. **1**, **2**, and **3** each involve Co(II) bound to two *N*,*O*-bidentate ligands with a distorted tetrahedral coordination sphere; **4** involves Co(III) bound to three *N*,*O*-bidentate ligands in a *mer*-N_3O_3 distorted octahedral geometry. $[Co^{II}(^{R}L)_2]$ (R = Ph or PhOMe) undergo two, one-electron, oxidations. The products of the first oxidation, $[\mathbf{1}]^+$ and $[\mathbf{2}]^+$, have been synthesised by the chemical oxidation of **1** and **2**, respectively; these cations, formulated as $[Co^{II}(^{R}L^{\bullet})(^{R}L)_2]^+$, comprise one phenoxyl radical and one phenolate ligand bound to Co(II) and are the first phenoxyl radical ligand complexes of tetra-coordinated Co(II). **4** undergoes two, one-electron, ligand-based oxidations, the first of which produces $[\mathbf{4}]^+$, $[Co^{III}(^{Bz}L^{\bullet})(^{Bz}L)_2]^+$. Unlike $[\mathbf{1}]^+$ and $[\mathbf{2}]^+$, product of the one-electron oxidation of $[Co^{II}(^{Bz}L)_2]$, $[\mathbf{3}]^+$, is unstable and decomposes to produce $[\mathbf{4}]^+$. These studies have demonstrated that the chemical properties of $[M^{II}(^{R}L^{\bullet})(^{R}L)_2]^+$ (M = Co, Cu, Zn) are highly dependent on the nature of both the ligand and the metal centre.

Introduction

There is much current interest in the nature and properties of d-transition metal complexes in which one or more of the ligands is present in a radical state.[1] This interest has been stimulated by spectroscopic studies of enzymes such as galactose oxidase (GAO),[2] glyoxal oxidase (GLO),[3] and ribonucleotide reductase (RNR),[4] that have shown the catalytic action to involve formation of a phenoxyl radical, either bound (GAO, GLO) or immediately adjacent (RNR), to a redox-active metal centre. Also, metal complexes, in which one (or more) of the ligands is a radical, possess novel physical properties.[5] Previously, we have shown that representatives of a family of pro-ligands (^{R}LH), each of which is comprised of an imidazole covalently bonded to an *o*,*p*-di-*tert*-butyl-substituted phenol (Scheme 1), can exist as a phenoxyl radical—as both $[^{R}LH^{\bullet}]^+$ and $[M^{II}(^{R}L^{\bullet})(^{R}L)]^+$ (M = Cu or Zn).[6] Herein, we report new developments of the coordination chemistry of this family of pro-ligands, ^{R}LH, for R = Ph, PhOMe, or Bz, with cobalt, including the synthesis and characterisation of Co(II) and Co(III) phenoxyl radical complexes.

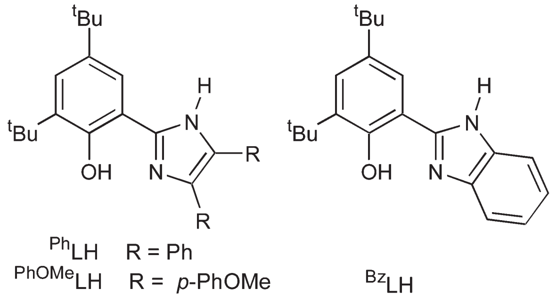

$[Co^{R}L_2]$ = R = Ph, **1**; R = PhOMe, **2**; R = Bz, **3** ; **4** = $[Co^{Bz}L_3]$

Scheme 1

Experimental

Unless stated otherwise, all manipulations were carried out at ambient temperature under an atmosphere of Ar using standard Schlenk techniques. Anhydrous MeOH, over molecular sieves, and $Co(BF_4)_2\cdot 6H_2O$ were purchased from Aldrich Chemical Company and used as received. Dry CH_2Cl_2, for both syntheses and electrochemical experiments, was freshly distilled under N_2 from CaH_2.

Syntheses of ^{R}LH (R = Ph, PhOMe, or Bz)

The synthesis of ^{Ph}LH has been reported previously.[6]

$^{PhOMe}LH$. (2-(2′-(4′,6′-Di-*tert*-butyl-2′-hydroxyphenyl)-4,5-bis-(*p*-methoxyphenyl)imidazole). A mixture of 3,5-di-*tert*-butylhydroxybenzaldehyde (1.0 g, 8.8 mmol), 4,4′-dimethoxybenzil (1.2 g, 8.6 mmol), and ammonium acetate (2.6 g, 32.0 mmol) were refluxed in glacial acetic acid (15 cm^3) until a precipitate formed (2–3 days). The reaction mixture was cooled to room temperature and H_2O (*ca.* 30 cm^3) was added to complete the precipitation. The yellow/green solid was collected by filtration, washed with H_2O (3 × 10 cm^3), dissolved in CH_2Cl_2 and the solution was dried over anhydrous $MgSO_4$. The $MgSO_4$ was removed by filtration and the filtrate evaporated to dryness. The resultant solid was dissolved in the minimum volume of CH_2Cl_2 and purified by flash chromatography on a silica gel column using CH_2Cl_2–pentane (6 : 4) as the eluant. Evaporation of the solvent produced a pale yellow powder; recrystallisation of this powder by the addition of hexane to a CH_2Cl_2 solution gave $^{PhOMe}LH$ as a white crystalline solid. Yield 2.0 g (45%). Elemental analysis: Calc. for $C_{31}H_{36}N_2O_3$: C 76.86, H 7.44, N 5.78; Found C 76.69, H 7.75, N 5.72%. ^1H-NMR (300 MHz, $CDCl_3$) δ 1.47 (s, 9H, ^tBu), 1.62 (s, 9H, ^tBu), 3.83 (s, 3H, OMe), 3.88 (s, 3H, OMe), 6.86 (d, 2H, *J* 9.4 Hz, $Ar_{OMe}H$), 6.97 (d, 2H, *J* 9.4 Hz, $Ar_{OMe}H$), 7.23 (d, 1H,

DOI: 10.1039/b410934a

---

† Electronic supplementary information (ESI) available: Figs. SI1–SI4 and Table SI1. See http://www.rsc.org/suppdata/dt/b4/b410934a/

J 2.5 Hz, Ar$_{OH}$H), 7.34 (d, 1H, *J* 2.5 Hz, Ar$_{OH}$H), 7.43 (d, 2H, *J* 9.4 Hz, Ar$_{OMe}$H), 7.59 (d, 2H, *J* 9.4 Hz, Ar$_{OMe}$H), 9.12 (s, 1H, OH/NH), 13.2 (s, 1H, OH/NH). ^{13}C-NMR (75 MHz, CDCl$_3$): δ 29.54, 31.64, 34.32, 35.26, 55.28, 111.68, 113.88, 114.32, 117.30, 123.11, 125.06, 126.39, 128.38, 129.74, 134.54, 137.35, 140.25, 146.27, 154.39, 158.72, 159.47. M.p. 245 °C. Positive FAB-MS: *m*/*z* 485 {(M + 1)$^+$}. UV/vis (CH$_2$Cl$_2$) λ_{max}/nm (ε/dm^3 mol^{-1} cm^{-1}): 232 (26180), 285 (27180), 323 (26175).

^{Bz}LH. (2-(3′,5′-Di-*tert*-butyl-2′-hydroxyphenyl)-benzimidazole). 3,5-Di-*tert*-butyl-salicylic acid (10.00 g, 40.0 mmol), phenol (4.14 g, 44.0 mmol), and *N*,*N*′-dicyclohexylcarbodiimide (11.87 g, 57.5 mmol) were dissolved in dry THF (240 cm^3) and stirred under N$_2$ for 4 days. The precipitate was removed from the mixture by filtration and washed with diethyl ether (3 × 10 cm^3) and the washings added to the filtrate. The volatile components were removed from the filtrate on a rotary evaporator and then *in vacuo*, to yield a peach coloured oil. Flash chromatography on silica gel, using pentane as the eluant, followed by evaporation of the solvent, produced phenyl-3,5-di-*tert*-butyl-2-hydroxybenzoate as a white powder. Yield 5.39 g (41.3%). Elemental analysis: Calc. for $C_{21}H_{26}O_3$: C 77.27, H 8.03; Found C 76.43, H 8.12%. ^{1}H-NMR (300 MHz, CDCl$_3$) δ 1.34 (s, 9H, ^{t}Bu), 1.44 (s, 9H, ^{t}Bu), 7.20 (d, 2H, *J* 7.5 Hz, Ar–H), 7.30 (t, 1H, *J* 7.5 Hz, Ar–H), 7.45 (t, 2H, *J* 7.5 Hz, Ar–H), 7.61 (d, 1H, *J* 2.5 Hz, Ar–H), 7.94 (d, 1H, *J* 2.5 Hz, Ar–H), 11.11 (s, 1H, –OH). M.p. 84–85 °C. Positive EI-MS: *m*/*z* 326 {M$^+$}.

Phenyl-3,5-di-*tert*-butyl-2-hydroxybenzoate (4.61 g, 14.1 mmol) and 1,2-phenylenediamine (1.53 g, 14.2 mmol) were refluxed for 3 h and the mixture then allowed to cool to room temperature. The resulting brown/black solid was dissolved in the minimum volume of CH$_2$Cl$_2$ and purified by flash chromatography on a silica gel column, using a CH$_2$Cl$_2$: hexane (2 : 3) as the eluant; evaporation of the solvent yielded a cream coloured solid. This solid was dissolved in CH$_2$Cl$_2$ and diffusion of hexane led to the precipitation of a white powder that was collected by filtration, washed with hexane (3 × 10 cm^3), and dried *in vacuo* to give ^{Bz}LH as a fluffy white solid. Yield 3.96 g (87%). Elemental analysis: Calc. for $C_{21}H_{26}N_2O$: C 78.23, H 8.13, N 8.69; Found C 77.91, H 8.13, N 8.78%. ^{1}H-NMR (300 MHz, CDCl$_3$) δ 1.30 (s, 9H, ^{t}Bu), 1.44 (s, 9H, ^{t}Bu), 7.21 (m, 4H, Bzim), 7.37 (d, 1H, *J* 2.5 Hz, Ar–H), 7.44 (d, 1H, *J* 2.5 Hz, Ar–H), 7.66 (s, 1H, OH/NH) and 10.04 (s, 1H, OH/NH). ^{13}C-NMR (75 MHz, CDCl$_3$) δ 29.53, 31.58, 34.36, 35.33, 111.13, 118.67, 123.1, 126.86, 137.83, 140.53, 152.52, 155.90. M.p. 215–219 °C. Positive EI-MS: *m*/*z* 322 {M$^+$}. UV/vis (CH$_2$Cl$_2$) containing [^{n}Bu$_4$N][BF$_4$] (0.4 M)) λ_{max}/nm (ε/dm^3 mol^{-1} cm^{-1}): 222 (42300), 242 (17400), 250 (11200), 266 (9100), 278 (12200), 290 (17700), 298 (25400), 325 (21200).

Syntheses of [Co(^{R}L)$_2$]

[Co(^{Ph}L)$_2$] (1). Addition of ^{Ph}LH (0.100 g, 0.24 mmol) in MeOH (10 cm^3) to a stirred solution of Co(BF$_4$)$_2$·6H$_2$O (0.040 g, 0.12 mmol) in MeOH (2 cm^3) produced an orange solution. Et$_3$N was then added dropwise until a red coloration persisted. This solution was stored at −30 °C for one week and an orange crystalline powder precipitated. The product was collected by filtration, washed (MeOH), and then dried *in vacuo* to afford **1**·2MeOH as an orange solid. Yield: 0.092 g (81%). Elemental analysis: Calc. for $C_{58}H_{62}N_4O_2Co\cdot 2MeOH$: C 74.30, H 7.27, N 5.78; Found: C 74.54, H 6.94, N 5.83. Positive FAB-MS: *m*/*z* 906 {(M + H)$^+$}. UV/vis (CH$_2$Cl$_2$): λ_{max}/nm (ε/dm^3 mol^{-1} cm^{-1}): 420–440 sh (747), 533 (171), 587 sh (103), *ca.* 900 (29).

Evaporation of a solution of **1**·2MeOH in MeCN afforded pink, rectangular, block-like, single crystals of **1**·2.5MeCN.

[Co(^{PhOMe}L)$_2$] (2). A solution of ^{PhOMe}LH (0.100 g, 0.21 mmol) in MeOH (10 cm^3) was added to a solution of Co(BF$_4$)$_2$·6H$_2$O (0.035 g, 0.10 mmol) in MeOH (5 cm^3), Et$_3$N was then added, as described for **1**. The resultant red solution was stored at −30 °C for one week and an orange crystalline powder precipitated. This solid was collected by filtration, washed (MeOH), crushed and dried *in vacuo* to afford **2**·2MeOH as an orange powder. Yield: 0.090 g (80%). Elemental analysis: Calc. for $C_{62}H_{68}N_4O_6Co\cdot 2MeOH$: C 70.50, H 7.21, N 5.14; Found: C 70.11, H 6.86, N 5.20. Positive FAB-MS: *m*/*z* 1025 {(M)$^+$}. UV/vis (CH$_2$Cl$_2$): λ_{max}/nm (ε/dm^3 mol^{-1} cm^{-1}): 430–440 sh (649); 531 (213), *ca.*586 (136), *ca.* 900 (40).

Evaporation of a CH$_2$Cl$_2$/DMF (9 : 1) solution of **2**·2MeOH afforded red, tablet-like, single crystals of **2**·2DMF.

[Co(^{Bz}L)$_2$] (3). A solution of ^{Bz}LH (0.100 g, 0.31 mmol) in MeOH (10 cm^3) was mixed with a solution of Co(BF$_4$)$_2$·6H$_2$O (0.053 g, 0.16 mmol) in MeOH (2 cm^3), Et$_3$N was then added as described for **1**. The resultant red solution was stored at −30 °C for one week and an orange crystalline powder precipitated. This solid was collected by filtration, washed (MeOH), crushed and dried *in vacuo* to afford **3**·2MeOH as a red–brown powder. Yield: 0.089 g (75%). Elemental analysis: Calc. for $C_{42}H_{50}N_4O_2Co\cdot 2MeOH$: C 69.00, H 7.63, N 7.32; Found: C 69.33, H 7.00, N 7.40. Positive FAB-MS: *m*/*z* 702 {(M)$^+$}. UV/vis (CH$_2$Cl$_2$): λ_{max}/nm (ε/dm^3 mol^{-1} cm^{-1}): 436 sh (400), 517 (96), 569 (92), 589 (96), *ca.* 900(41).

Purple, tablet-like crystals of **3**·4MeOH were obtained on storing a solution of the compound, saturated at room temperature in MeOH at −30 °C.

[Co(^{Bz}L)$_3$] (4). Addition of a solution of Co(BF$_4$)$_2$·6H$_2$O (0.171 g, 0.50 mmol) in MeOH (10 cm^3) to ^{Bz}LH (0.500 g, 1.50 mmol) dissolved in MeOH (15 cm^3) produced a pink solution. Addition of a few drops of Et$_3$N and then *ca.* 5 cm^3 of 9% w/v H$_2$O$_2$ gave a brown solution. This solution was maintained at room temperature, stirred for 15 min and then allowed to stand for *ca.* 2 h, whence brown crystals were formed. The solid was collected by filtration, crushed, and dried *in vacuo* to afford a dark brown powder. Yield: 0.283 g (55%). Elemental analysis: Calc. for $C_{63}H_{75}N_6O_3Co$: C 73.95, H 7.39, N 8.22; Found: C 74.06, H 7.10, N 8.48. Positive FAB-MS: *m*/*z* 1022{M$^+$}. ^{1}H-NMR (300 MHz, CDCl$_3$): δ 0.61 (s, 9H, ^{t}Bu,), 0.73 (s, 9H, ^{t}Bu), 1.03 (s, 9H, ^{t}Bu), 1.09 (s, 9H, ^{t}Bu), 1.16 (s, 9H, ^{t}Bu), 1.23 (s, 9H, ^{t}Bu), 6.31–7.62 (m, 18H, ArH and BzH), 10.07 (s, 1H, NH), 10.32 (s, 1H, NH), 10.73 (s, 1H, NH). UV/vis (CH$_2$Cl$_2$): λ_{max}/nm (ε/dm^3 mol^{-1} cm^{-1}): 473 sh (1860), 610 (490), 714 nm (310).

Slow evaporation of a DMF : CH$_2$Cl$_2$ (9 : 1) solution of this solid yielded brown, block-like crystals of **4**·4DMF.

Syntheses of [1][BF$_4$] and [2][PF$_6$]

[1][BF$_4$]. A solution of **1**·2MeOH (0.250 g, 0.26 mmol) in dry CH$_2$Cl$_2$ (40 cm^3) was transferred into a pre-cooled (−10 °C) stirred suspension of Ag[BF$_4$] (0.054 g, 0.28 mmol) in dry CH$_2$Cl$_2$ (5 cm^3) that was protected from light. An intensely coloured green solution resulted and a silver mirror was deposited on the sides of the reaction vessel. The reaction mixture was stirred at −10 °C for 1 h, then allowed to warm to room temperature and stirred for a further 10 min. Filtration, followed by evaporation of the solvent, gave a dark green solid. This solid was dissolved in a minimum volume of CH$_2$Cl$_2$; diffusion of pentane to this solution at −40 °C, followed decantation of the mother liquor from the precipitate, afforded [**1**][BF$_4$] as a dark green solid. Yield: 0.200 g (79%). Elemental analysis: Calc. for $C_{58}H_{62}N_4O_2CoBF_4$: C 70.93, H 6.36, N 5.71; Found: C 70.18, H 6.38, N 5.39. Positive FAB-MS ion at *m*/*z* 905{M$^+$}. UV/vis (CH$_2$Cl$_2$): λ_{max}/nm (ε/dm^3 mol^{-1} cm^{-1}): 232(70,800), 291(40,900), 350(30,000), 529(200), 583(100), 450(500).

[2][PF$_6$]. **2**·2MeOH (0.555 g, 0.51 mmol) in dry CH$_2$Cl$_2$ (40 cm^3) and Ag[PF$_6$] (0.137 g, 0.54 mmol) in dry CH$_2$Cl$_2$ (5 cm^3) and were reacted as described for [**1**][BF$_4$]. The resultant dark green solid was washed with Et$_2$O, to remove the unreacted **2**

and then recrystallised by the slow diffusion of pentane into a CH_2Cl_2 solution at −40 °C; this yielded a dark green crystalline powder. The mother liquor was removed and the powder dried *in vacuo* to give [**2**][PF_6]. Yield: 0.416 g (70%). Positive FAB-MS ion at *m*/*z* 1026 {$(M + H)^+$}. Elemental analysis: Calc. for $C_{62}H_{70}N_4O_6CoPF_6$: C 63.58, H 6.02, N 4.79; Found: C 63.42, H 5.90, N 4.71. Positive FAB-MS ion at *m*/*z* 1026{$(M + H)^+$}. UV/vis: λ_{max}/nm (ε/dm^3 mol^{-1} cm^{-1}): 390(11330), 409 sh (10200), 589 nm (8760), residual absorption 750–900 nm (*ca.* 4000).

Physical methods

Elemental analyses of the compounds isolated in these studies were accomplished by the Microanalytical Laboratory of the School of Chemistry, of the University of Nottingham. FAB and EI mass spectra were recorded on a Fisons VG Trio 200 or a Fisons VG Autospec spectrometer, NMR spectra were recorded on a Bruker DPX300 NMR spectrometer, and UV/vis spectra were recorded on a Perkin Elmer Lambda 5 spectrophotometer.

The cyclic voltammogram of each compound (1 mM) in CH_2Cl_2, containing [NBu^n_4][BF_4] (0.4 M) as the background electrolyte, was recorded at room temperature using a glassy carbon or Pt wire working electrode, a Pt wire secondary electrode, and a saturated calomel reference electrode. The cyclic voltammogram of each compound was referenced to the $[Fc]^+/[Fc]$ couple that was used as the internal standard. When necessary, to avoid overlapping redox couples, the $[FeCp*_2]^+/[FeCp*_2]$ couple was used as the internal reference and the potentials of the redox process(es) observed were referenced to that of the $[Fc]^+/[Fc]$ couple by an independent calibration ($\Delta E_{1/2}$, $[Fc]^+/[Fc]$ *vs.* $[FeCp*_2]^+/[FeCp*_2]$, = 0.526 V). All coulometric measurements were performed at 273 K in a CH_2Cl_2 solution containing [NBu^n_4][BF_4] (0.4 M); the cell consisted of a Pt/Rh gauze basket working electrode, a Pt/Rh gauze secondary electrode, and a saturated calomel reference electrode. Both CV and CPE measurements were performed using an Autolab PGSTAT20 potentiostat.

UV/vis spectroelectrochemistry was accomplished for CH_2Cl_2 solutions containing [NBu^n_4][BF_4] (0.4 M) in an optically transparent electrochemical (OTE) cell (modified quartz cuvette, optical pathlength 0.5 mm). A three-electrode configuration was used in the cell, comprising a Pt/Rh gauze working electrode, a Pt wire secondary electrode contained in a fritted PTFE sleeve, and a saturated calomel electrode that was isolated from the test solution by a bridge tube containing the electrolyte solution retained by a porous frit. The potential at the working electrode was controlled by a Sycopel Scientific Ltd. DD10M potentiostat. UV/vis spectra were recorded on a Perkin Elmer Lambda 16 spectrophotometer; during the measurements the spectrometer cavity was purged with N_2 and temperature control at the sample was achieved by flowing cooled N_2 across the surface of the cell.

EPR spectra were recorded on a Bruker X-band EMX spectrometer. Magnetic fields and microwave frequencies were calibrated with a Bruker ER035M NMR gaussmeter and an EIP microwave counter, respectively.

Magnetic susceptibility data for **1**, **2**, **3**, [**1**][BF_4] and [**2**][PF_6] were recorded on a Quantum Design MPMS SQUID magnetometer at an applied field of 1 T and were corrected for core diamagnetism and contributions from the gelatine capsule sample holder.

Diffraction data for a single crystal of each of **1**·2.5MeCN, **2**·2DMF, **3**·4MeOH, and **4**·4DMF were collected on a Bruker SMART 1000 CCD area detector diffractometer equipped with an Oxford Cryosystem open-flow nitrogen cryostat[7] using ω-scans and graphite-monochromated Mo–Kα radiation (0.71073 Å). Data were corrected for Lorentz and polarization effects and absorption using a multi-scan method. The structure of **3**·4MeOH was solved by direct methods and those of **1**·2.5MeCN, **2**·2DMF, and **4**·4DMF by Patterson methods using SHELXS 97.[8] Each structure was refined against F^2 using SHELXL 97.[8] Unless otherwise stated, all non-H atoms were refined with anisotropic atomic displacement parameters (adps). The hydrogen atoms of: CH_3CN, CH_3OH, and $(CH_3)_2NCHO$, were located from difference Fourier syntheses and their positions refined as part of a rigid rotor. All other H atoms were placed in geometrically calculated positions and refined as part of a riding model, with $U(H)_{iso} = 1.2U_{eq}(C)$, for those of C_6H_5 and $U(H)_{iso} = 1.5U_{eq}(C)$, for those of CH_3. For **1**·2.5MeCN, a disordered ^{t}Bu group was modeled over two sites with occupancies of 0.7 and 0.3; suitable geometric restraints were applied and the C atoms were refined isotropically. Restraints were also applied to each MeCN molecule; the position of one of which is half-occupied. For **2**·2DMF, one disordered ^{t}Bu group was modeled over two half-occupied sites, with suitable restraints applied, and the C-atoms were refined isotropically. For **3**·4MeOH, the disorder of one oxygen atom of one MeOH molecule was modeled over two sites (O4s and O4s′) with occupancies of 0.4 and 0.6, respectively; C4s, O4s, and O4s′ were refined with isotropic adps—their H atoms and those of C3s could not be located. For **4**·4DMF, one disordered DMF molecule was modeled over two sites with occupancies of 0.7 and 0.3; O1SC and N1SC are common to both components and the C, N and O atoms were refined isotropically and restraints applied to their C–O and N–C distances. The hydrogen atoms of this DMF molecule were not located.

CCDC reference numbers 227296–227299.

See http://www.rsc.org/suppdata/dt/b4/b410934a/ for crystallographic data in CIF or other electronic format.

Results and discussion

Nature of [Co(^{R}L)$_2$] (1, 2, and 3) and [Co(^{Bz}L)$_3$] (4)

The pro-ligand ^{PhOMe}LH was synthesised in a similar manner to that[6] for ^{Ph}LH by the condensation of 3,5-di-*tert*-butylhydroxybenzaldehyde with 4,4′-dimethoxybenzil (1 : 1) in AcOH in the presence of an excess of [NH_4][OAc]. In contrast, ^{Bz}LH, was prepared by the condensation of the phenyl ester derivative of the 3,5-di-*tert*-butyl-salicylic acid and 1,2-phenylenediamine.

$Co(BF_4)_2{\cdot}6H_2O$ reacted with each of the pro-ligands ^{R}LH (1 : 2) in the presence of Et_3N to form the corresponding [Co(^{R}L)$_2$] compound (Scheme 1; R = Ph, **1**; R = PhOMe **2**; R = Bz, **3**). $Co(BF_4)_2{\cdot}6H_2O$ reacts with ^{Bz}LH (1 : 3) and H_2O_2 in the presence of Et_3N to form [Co(^{Bz}L)$_3$] (**4**).

1·2.5MeCN, **2**·2DMF, **3**·4MeOH, and **4**·4DMF have been characterised by X-ray crystallography (Fig. 1, Table 1). In each compound solvent molecules form hydrogen bonds to the phenolate and/or imidazole groups of the ligands. The atom possessing a lone pair of electrons (MeC*N*, Me*O*H, or DMF(*O*)) forms an *O*(*N*)···H–N hydrogen bond to the imidazole N–H group; also, for **3**·4MeOH, MeO*H* forms a hydrogen bond to one of the coordinated phenolate oxygen atoms (Table SI1, see ESI†).

In **1**·2.5MeCN, **2**·2DMF, and **3**·4MeOH the two *N*,*O*-bidentate ligands form a distorted tetrahedral N_2O_2-coordination sphere about the Co (Fig. 1); the angle between the Co(1)N(5)O(1) and Co(1)N(5A)O(1A) planes is 90 ± 5°. The lengths of the C–C, C–N, and C–O bonds in **1**·2.5MeCN, **2**·2DMF, **3**·4MeOH, and **4**·4DMF correspond to each ligand being present as the L^- anion.[6] In particular, the length of the C–O bond of each ligand (1.317(5)–1.337(6) Å) is characteristic of a phenolate and is distinct from that (1.264(5) Å) of the phenoxyl radical $^{Ph}L^{\cdot}$ in [Cu^{II}($^{Ph}L^{\cdot}$)(^{Ph}L)][BF_4];[6] and those of other structurally characterised phenoxyl radical complexes.[9] The lengths (Table 2) of the Co–O (1.905(3)–1.938(4) Å) and Co–N (1.960(4)–1.998(2) Å) bonds of **1**·2.5MeCN, **2**·2DMF, and **3**·4MeOH are in agreement with those of the corresponding bonds of other[10,11] [Co^{II}(*NO*)$_2$] complexes, *e.g.* [Co^{II}(L′)$_2$] (L′H = *N*-ethyl-2-(2′-hydroxy-3′-methylphenyl)–benzimidazole) with Co–O of 1.922(8) Å and

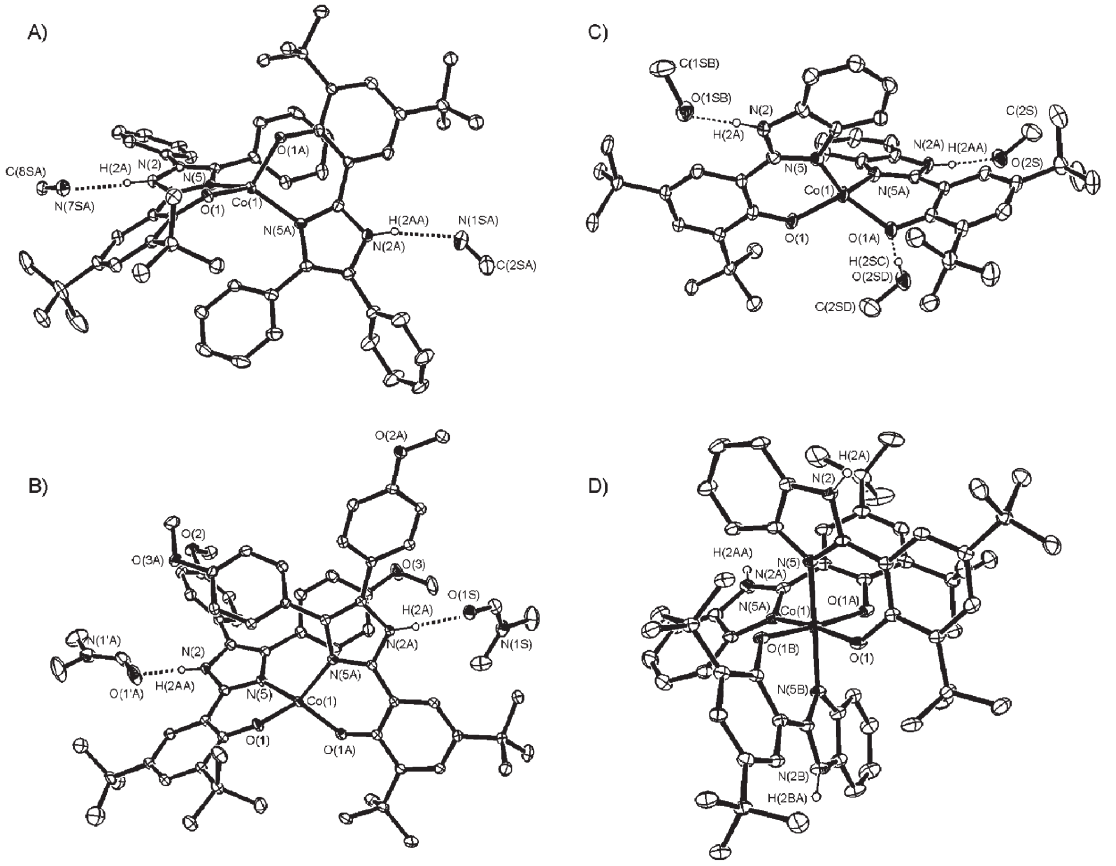

Fig. 1 ORTEP representations of the molecular structures of (A) **1** in **1**·2.5MeCN, (B) **2** in **2**·2DMF, (C) **3** in **3**·4MeOH and (D) **4** in **4**·4DMF. Only the solvent molecules that are involved in hydrogen bonding interactions with the complex are shown; however, for clarity these are not shown for **4**·4DMF.

Co–N of 1.979(3) Å.[10] In **3**·4MeOH the Co(1)–O(1A) bond (1.938(4) Å) is slightly longer than the Co(1)–O(1) (1.905(3) Å) bond and the Co–O bonds of **1**·2.5MeCN and **2**·2DMF (1.910(2)–1.916(2) Å); this difference is attributed to the presence of the O(1A)···H(2SC) hydrogen bond in **3**·4MeOH (Fig. 1C, Table SI1, see ESI†).

The UV/vis spectra of a solution of **1**, **2**, and **3** in CH_2Cl_2 are similar and each is typical of a tetrahedral Co(II) (d^7, $S = 3/2$) centre; each involves two/three d → d transitions between 500 and 600 nm ($\varepsilon \sim 100–250$ dm^3 mol^{-1} cm^{-1}), plus a shoulder at 420–440 nm ($\varepsilon \sim 400–800$ dm^3 mol^{-1} cm^{-1}) (Fig. SI2 and Table SI2, see ESI†) that is attributed to a phenolate → Co(II) charge transfer transition.[12]

1, **2**, and **3**, as a solid at *ca.* 298 K, each possesses a magnetic moment of 4.2–4.6 BM, consistent with a tetrahedral Co(II) ($S = 3/2$) centre with contributions from spin–orbit coupling as indicated by a relatively large zero field splitting (see ESI†, Fig. SI1).‡ However, **1**, **2**, and **3** are EPR silent in CH_2Cl_2 solution at 298 K, presumably because of rapid spin–lattice relaxation of the Co(II) (d^7, $S = 3/2$) centre.

4·4DMF involves three *N*,*O*-bidentate ligands that produce a distorted *mer*-N_3O_3–octahedral coordination sphere about the Co (Fig. 1D). This inner coordination sphere is analogous to that of $[Co^{III}(L')_3]$[10] and other $[Co^{III}(N,O)_3]$ complexes[13] and involves Co–O and Co–N bonds of length 1.887(3)–1.914(3) Å and 1.914(4)–1.944(3) Å, respectively (Table 3). The geometry at the Co centre approximates to that of an octahedron with *cis*- and *trans*-*N*(*O*)–Co–*N*(*O*) interbond angles that range from 84.16(14) to 93.63(14)° and from 173.06(14) to 175.77(13)°, respectively (Table 3). Each imidazole N–H group is hydrogen bonded to the carbonyl group of a DMF molecule (Table SI1, see ESI†).

4 is considered to involve a Co(III), d^6 low spin ($S = 0$) centre bound to three $^{Bz}L^-$ ligands. Thus, **4** is diamagnetic in the solid state and EPR silent in CH_2Cl_2 solution. In $CDCl_3$ solution, **4** exhibits a well resolved ^{1}H-NMR spectrum (Fig. SI3, see ESI†) that is consistent with the distorted octahedral geometry observed for **4**·4DMF being maintained in solution. The spectrum comprises six resonances between 0.6 and 1.2 ppm, assigned to ^{t}Bu singlets, and three resonances between 10.0 and 10.7 ppm, assigned to N–H singlets. The UV/vis spectrum of **4** in CH_2Cl_2 solution at *ca.* 298 K manifests absorptions at λ_{max}/nm (ε/dm^3 mol^{-1} cm^{-1}) 473 sh (1860), 610 (490), and 714 (310).

The above observations indicate that the molecular structures of **1**, **2**, **3** and **4**, identified in the solid state, are retained in solution.

Redox properties of 1 and 2 and the nature of [1]$^+$ and [2]$^+$

The cyclic voltammograms of **1** and **2**, in CH_2Cl_2 at *ca.* 298 K (Fig. 2) each exhibit two, one-electron (as determined by coulometry) oxidations. The first oxidation process is electrochemically reversible (Fig. 2a) whereas the second oxidation

---

‡ The data obtained for **1**, **2**, and **3** were analysed on the basis of a spin-Hamiltonian description of the electronic ground state: $H_1 = D_{Co}[\boldsymbol{S}_z^2 - S(S+1)/3 + (E_{Co}/D_{Co})(\boldsymbol{S}_X^2 - \boldsymbol{S}_Y^2)] + \mu_B g_{Co} \boldsymbol{B}\cdot\boldsymbol{S}$; where $S = 3/2$ is the spin of the metal ion and D_{Co}, E_{Co}/D_{Co}, and g_{Co} are the local axial and rhombic zero-field parameters and *g*-values, respectively. For all simulations the E_{Co}/D_{Co} value was not significantly determined and was therefore fixed to zero. The temperature dependence (3–320 K) of the magnetic moments of **2** and **3** were successfully interpreted on this basis. (Fig. SI1(b), see ESI†). However, in respect of the temperature dependence (3–320 K) of the magnetic moment of **1**, the consideration of **1** composed of isolated $[Co(^{Ph}L)_2]$ molecules only fits the data observed between 200 and 300 K (Fig. SI1(a), see ESI†). The lack of agreement between the experimental and simulated data at a lower temperature (the maximum discrepancy is at *ca.* 50 K) is characteristic of solid state interactions between the Co(II) centres. The plot of $1/\chi$ *vs.* temperature (see Fig. SI1(a) inset, see ESI†) is linear at high temperature (above 100 K), but at lower temperature shows a deviation from the Curie law with a Weiss temperature of 10 K. This deviation is typically indicative of the presence of intermolecular ferromagnetic interactions (see Fig. SI1(a) inset, see ESI†).

Table 1 Crystallographic data for **1**·2.5MeCN, **2**·2DMF, **3**·4MeOH, **4**·4DMF

	1·2.5MeCN	**2**·2DMF	**3**·4MeOH	**4**·4DMF
Empirical formula	$CoC_{63}H_{69.5}N_{6.5}O_2$	$CoC_{68}H_{84}N_6O_8$	$CoC_{46}H_{66}N_4O_6$	$CoC_{75}H_{103}N_{10}O_7$
M	1008.68	1172.34	829.96	1315.60
Crystal system	Monoclinic	Triclinic	Monoclinic	Monoclinic
Space group (no.)	$P2_1/n$	$P\bar{1}$	$P2_1/c$	$C2/c$
a/Å	16.8711(12)	12.0122(8)	16.725(4)	25.561(2)
b/Å	17.8112(13)	13.1107(9)	10.589(3)	12.9720(10)
c/Å	19.2944(14)	22.193(2)	25.658(6)	44.240(3)
a/°	90	103.221(2)	90	90
β/°	101.626(1)	96.280(2)	93.876(6)	100.116(10)
γ/°	90	111.092(2)	90	90
V/Å^3	5678.9(7)	3103.0(6)	4534.0(3)	14440.9(19)
Z	4	2	4	8
T/K	150(2)	150(2)	150(2)	150(2)
D_c/g cm^{-3}	1.17	1.25	1.22	1.21
μ/mm^{-1}	0.350	0.337	0.430	0.297
Reflections collected	37003	26386	24799	59973
Independent reflections (R_{int})	13989 (0.092)	13916 (0.02)	10856 (0.132)	16845 (0.072)
Observed reflections [$I > 2\sigma(I)$]	5847	10794	3908	10626
R	0.0623	0.0656	0.076	0.0855
R_w	0.1781	0.1353	0.224	0.1312

Table 2 Selected bond lengths (Å) and angles (°) for **1**·2.5MeCN and **2**·2DMF and **3**·4MeOH

	1·2.5MeCN	**2**·2DMF	**3**·4MeOH
Co(1)–O(1A)	1.916(2)	1.914(2)	1.938(4)
Co(1)–O(1)	1.911(2)	1.910(2)	1.905(3)
Co(1)–N(5A)	1.985(3)	1.997(2)	1.994(4)
Co(1)–N(5)	1.991(3)	1.998 (2)	1.960(4)
O(1A)–Co(1)–O(1)	109.58(1)	117.19(7)	118.2 (2)
N(5A)–Co(1)–N(5)	126.10(11)	112.41(7)	126.0(2)
O(1A)–Co(1)–N(5)	118.34 (12)	122.63(7)	117.6(2)
O(1)–Co(1)–N(5A)	115.63(12)	118.61(7)	114.4(2)
O(1A)–Co(1)–N(5A)	93.39(11)	94.12(6)	90.1 (2)
O(1)–Co(1)–N(5)	94.47(11)	93.88(7)	93.0(2)

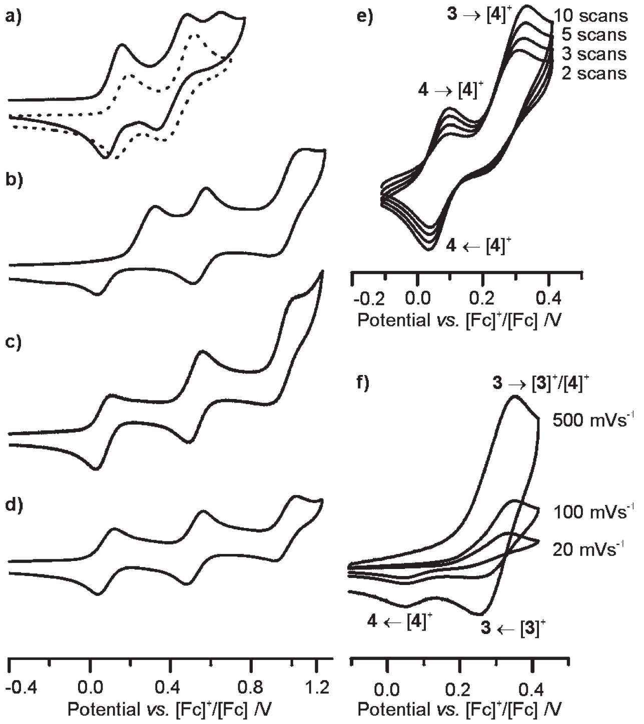

Fig. 2 Cyclic voltammograms of: (a) **1** (dotted line) and **2** (solid line); (b) **3** ; (c) one-electron oxidized solution of **3** recorded at a Pt wire; (d) **4**; (e) **3** at 100 mV s^{-1}; (f) **3** performed at scan-rates of 20, 100 and 500 mV s^{-1}.

process is not. The potential of each oxidation process is very similar to that of the corresponding oxidation of the analogous [M(^{R}L)$_2$] (M = Cu or Zn) compound[6,14] (Table 4). Therefore, we consider that each of these oxidations is ligand-based. UV/vis spectroelectrochemistry for the first oxidation of **1** and **2** shows that this process is chemically reversible and UV/vis absorption spectra of [**1**]$^+$ and [**2**]$^+$ (Fig. 3) show a band at *ca.* 410 nm (λ_{max}/nm (ε/M^{-1}cm^{-1}) 408 (9700) [**1**]$^+$; 409 (10200) [**2**]$^+$), the wavelength and intensity of which is typical of a π–π* transition of a phenoxyl radical (L$^\bullet$).[6,5a]

[**1**]$^+$ and [**2**]$^+$ have been synthesised by the oxidation of the parent compound with Ag$^+$ (1 : 1); **1** was treated with Ag[BF$_4$] and **2** with Ag[PF$_6$]. The products of these oxidations, [**1**][BF$_4$] and [**2**][PF$_6$], are inert for several days at room temperature, both as crystalline powders exposed to air and in CH_2Cl_2 solution under an Ar or N_2 atmosphere. The temperature dependence of the magnetic moments of [**1**][BF$_4$] and [**2**][PF$_6$], from 3 to 320 K (Fig. 4), have been modelled successfully by the Hamiltonian $H = H_1 + \mu_B g_{rad} \boldsymbol{B}\cdot\boldsymbol{S}_{rad} - 2J\boldsymbol{S}_{Co}\boldsymbol{S}_{rad}$ ($H_1 = D_{Co}[\boldsymbol{S}_z^2 - S(S+1)/3 + (E_{Co}/D_{Co})(\boldsymbol{S}_X^2 - \boldsymbol{S}_Y^2)] + \mu_B g_{Co} \boldsymbol{B}\cdot\boldsymbol{S}$). In both cases, the local spin of the Co(II) centre (S_{Co}) is 3/2 and that of the radical ligand (S_{rad}) is 1/2; J represents the exchange coupling constant and is <-250 cm^{-1} for [**1**][BF$_4$] and $= -198$ cm^{-1} for [**2**][PF$_6$] (Fig. 4). Thus, the magnetic data are consistent with both [**1**][BF$_4$] and [**2**][PF$_6$] possessing an $S = 1$ ground state arising from a strong antiferromagnetic coupling between the Co(II) and the phenoxyl radical centres. The D values for [**1**][BF$_4$] and [**2**][PF$_6$] ($D_{Co} = -24.5 \pm 2.0$ and $D_{Co} = -13.7 \pm 2.0$ cm^{-1}, respectively, Fig. 4) are comparable to those of **1** and **2** ($D_{Co} = -24.5 \pm 2.0$ and $D_{Co} = -12.9 \pm 2.0$ cm^{-1}, respectively, Fig. SI1, see ESI†). This suggests that there are no substantial changes in geometry about the Co centres of **1** and **2** on oxidation. The failure to detect an EPR signal for [**1**][BF$_4$] and [**2**][PF$_6$] (at 4 and 77 K, at X- and Q-band frequencies, both as a solid and in CH_2Cl_2 solution) is consistent with the cations possessing a $S = 1$ ground state, in which the $\Delta M_s = \pm 1$ transitions cannot be observed due to a relatively high zero-field splitting.

Oxidation of 4 and 3

The cyclic voltammogram of **4** (Fig. 2d) manifests three oxidation processes. Coulometric studies show that the first and second oxidations are each one-electron processes and UV/vis OTE investigations indicate that these are chemically reversible. The first and second oxidation (Fig. 5) processes are accompanied by the growth of a relatively strong absorption at 503 nm (ε = 4420 dm^3 mol^{-1} cm^{-1}) and 530 nm (ε = 7200 dm^3 mol^{-1} cm^{-1}) for [**4**]$^+$ and [**4**]$^{2+}$, respectively. These

Table 3 Selected bond lengths (Å) and angles (°) for **4**·2DMF

4·4DMF			
Co(1)–O(1)	1.894(3)	N(5A)–Co(1)–N(5B)	88.94(15)
Co(1)–O(1A)	1.914(3)	O(1)–Co(1)–N(5)	91.37(13)
Co(1)–O(1B)	1.887(3)	O(1)–Co(1)–N(5A)	173.06(14)
Co(1)–N(5)	1.944(3)	O(1)–Co(1)–N(5B)	84.16(14)
Co(1)–N(5A)	1.914(4)	O(1A)–Co(1)–N(5)	90.45(14)
Co(1)–N(5B)	1.924(3)	O(1A)–Co(1)–N(5A)	90.83(14)
		O(1A)–Co(1)–N(5B)	93.63(14)
O(1)–Co(1)–O(1A)	88.83(13)	O(1B)–Co(1)–N(5)	85.32(14)
O(1)–Co(1)–O(1B)	91.29(13)	O(1B)–Co(1)–N(5A)	89.56(14)
O(1A)–Co(1)–O(1B)	175.77(13)	O(1B)–Co(1)–N(5B)	90.59(14)
N(5)–Co(1)–N(5A)	−95.56(14)		
N(5)–Co(1)–N(5B)	−173.88(15)		

Table 4 Cyclic voltammetric data for the oxidation processes of $[\mathrm{Co}(^{R}L)^{2}]$ (R = Ph, PhOMe or Bz) and $[\mathrm{Co}(^{Bz}L)_3]$ at 100 mV s^{-1}. All potentials are expressed *vs.* $[\mathrm{Fc}]^+/[\mathrm{Fc}]$

Complex	First oxidation E/V(ΔE/mV)	Second oxidation E/V(ΔE/mV)	ΔE $[\mathrm{Fc^*}]^+/[\mathrm{Fc^*}]$/mV
1	0.16(80)[a]	0.51	70
2	0.12(80)[a]	0.49	80
3	0.35[b]	—	80
4	0.08(80)[a]	0.52(90)[a]	90

[a] $E_{½}$ for a reversible redox process. [b] $E_p{}^a$.

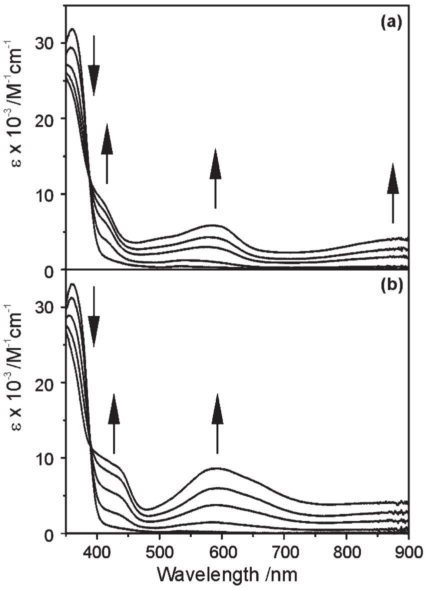

Fig. 3 UV/vis spectroelectrochemistry for the one-electron oxidation of (a) **1** and (b) **2** in CH_2Cl_2 at 273 K.

are similar to the bands observed for $[\mathrm{Cu^{II}}(^{Bz}L^{\bullet})(^{Bz}L)]^+$ and $[\mathrm{Zn^{II}}(^{Bz}L^{\bullet})(^{Bz}L)]^+$.[14] Thus, $[\mathbf{4}]^+$ is considered to be constituted as $[\mathrm{Co^{III}}(^{Bz}L^{\bullet})(^{Bz}L)_2]^+$ with a phenoxyl radical ($^{Bz}L^{\bullet}$) and two phenolates (^{Bz}L) coordinated to Co(III). The X-band EPR spectrum of $[\mathbf{4}]^+$, generated electrochemically from **4** in fluid CH_2Cl_2 solution at room temperature and then cooled to 175 K (Fig. SI4, see ESI†), consists of a broad (*ca.* 40 G) signal centred at $g = 2.016$. The line width of this signal excludes the possibility of a large hyperfine coupling (*e.g.* >10 G) with the ^{59}Co nucleus ($I = 7/2$). This result is in agreement with EPR data obtained for other Co(III)–radical ligand complexes, for which $A(^{59}\mathrm{Co})$ values <12.5 G have been observed.[15–18]

3 undergoes a facile, one-electron chemically irreversible oxidation at $E_p{}^a = 0.34$ V (*vs.* $[\mathrm{Fc}]^+/[\mathrm{Fc}]$) (Fig. 2b). The profile of the cyclic voltammogram for this process differs significantly from that observed for the first oxidation of **1** and **2** (Fig. 2a). The first oxidation of **3** is irreversible *and* $[\mathbf{4}]^+$ was the only

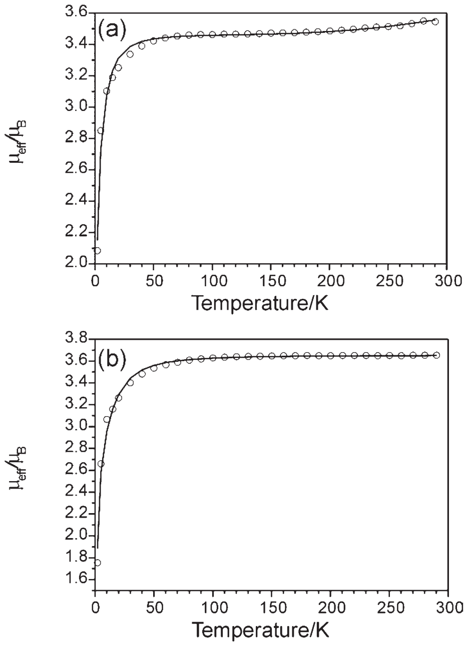

Fig. 4 Temperature dependence of the effective magnetic moment of (top) $[\mathbf{2}][\mathrm{PF_6}]$; the solid line represents the best fit by use of the parameters: $g_{\mathrm{Co}} = 2.360$, $g_{\mathrm{rad}} = 2.000$ (fixed), $D_{\mathrm{Co}} = -13.7 \pm 2.0$ cm^{-1} ($E_{\mathrm{Co}}/D_{\mathrm{Co}} = 0.08$), $J = -198$ cm^{-1}; and (bottom) $[\mathbf{1}][\mathrm{BF_4}]$; the solid line represents the best fit by use of the parameters: $g_{\mathrm{Co}} = 2.465$; $g_{\mathrm{rad}} = 2.000$ (fixed); $D_{\mathrm{Co}} = -24.5 \pm 2.0$ cm^{-1} ($E_{\mathrm{co}}/D_{\mathrm{co}} = 0.07$). For $[\mathbf{1}][\mathrm{BF_4}]$, the strong antiferromagnetic coupling results in a fit that shows little variation in quality for $J < -250$ cm^{-1}.

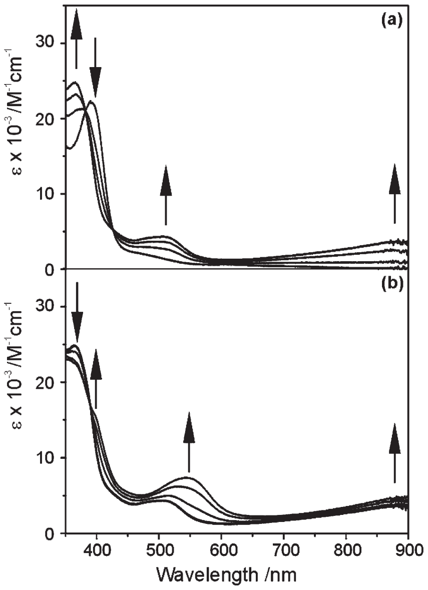

Fig. 5 UV/vis spectra for the (a) the one-electron oxidation and (b) the two-electron oxidation of **4** at 273 K.

product of the oxidation to be identified by UV/vis, EPR and cyclic voltammetric (*cf.* Figs. 2c and 2d) investigations of the electrolysed solution. At scan rates <100 mV s^{-1}, the first oxidation of **3**, in the reverse sweep, shows a reduction at a potential consistent with the process [**4**]$^+$ → [**4**]. Furthermore, multiple scan cyclic voltammetric studies of the first oxidation of **3** (Fig. 2e) indicate that the depletion of **3** is accompanied by the development of the [**4**]$^+$/[**4**] redox couple. However, at 500 mV s^{-1} (Fig. 4f) a new cathodic process at $E_p^c = 0.26$ V accompanies the anodic process at $E_p^a = 0.35$ V, that is assigned to a ligand-based [**3**]$^+$/[**3**] couple, by comparison with the first oxidation processes for **1**, **2** and the first oxidation of $[Cu(^{Bz}L)_2]$ ($E_{1/2} = 0.36$ V $\Delta E = 70$ mV).[14]

The above observations are consistent with a reaction sequence in which one-electron oxidation of [**3**] produces [**3**]$^+$, from which [**4**]$^+$ is produced. This behaviour is in marked contrast to the inertness of [**1**]$^+$ and [**2**]$^+$, each of which have been isolated and characterised. Also, $[Co^{II}(^{Bz}L)_2]^+$ is the only $[M^{II}(^{R}L)_2]^+$ complex of those so far investigated (M = Co, Cu,[6,14] or Zn;[6,14] R = Ph, PhOMe, or Bz) that is reactive. Our interpretations of these observations are: (i) for these complexes, oxidation of a Co(II) centre to produce Co(III) could occur, whereas this is not possible for Zn(II) and might not be favoured for Cu(II); (ii) the formation of Co(III) would be greatly encouraged by the addition of a (bidentate) ligand, to produce an octahedral, d^6, low-spin centre; (iii) the formation of a $[Co(^{R}L)_3]$ complex appears to be possible for R = Bz (Fig. 1D) but not for R = Ph or PhOMe under identical reaction conditions; the only product isolated from the reaction of $Co(BF_4)_2 \cdot 6H_2O$ with ^{R}LH (R = Ph or PhOMe) (1 : 3) is the corresponding $[Co^{III}(^{R}L)_2]$ complex (*i.e.* **1** or **2**, respectively). Thus, the steric hindrance induced by the 4,5-diphenyl–imidazole unit of ligand ^{R}LH (R = Ph or PhOMe) may explain the differences in the chemical properties of the radical complexes [**1**]$^+$ or [**2**]$^+$ as compared to [**3**]$^+$.

Conclusions

Three new $[Co^{II}L_2]$ complexes of the phenol–imidazole proligands ^{R}LH have been synthesised and characterised. Each of these complexes undergoes a one-electron, ligand-based, oxidation. The products of this oxidation $[Co^{II}(^{R}L^{\bullet})(^{R}L)]^+$ (R = Ph or PhOMe) are analogous to those reported previously for Cu and Zn[6,14] and represent the first phenoxyl radical ligand complexes of tetra-coordinated Co(II) presumably stabilized by the steric hindrance of the ligands. However, of the systems so far investigated, $[Co^{II}(^{Bz}L^{\bullet})(^{Bz}L)]^+$ is unique in being reactive to form $[Co^{III}(^{Bz}L^{\bullet})(^{Bz}L)_2]^+$, demonstrating that the chemical properties of such systems are dependent on the nature of both the phenoxyl radical and the metal centre.

Acknowledgements

We thank the EPSRC for financial support.

References

1 (*a*) P. Chaudhuri and K. Wieghardt, *Prog. Inorg. Chem.*, 2001, **50**, 151; (*b*) C. G. Pierpont, *Coord. Chem. Rev.*, 2001, **216–217**, 99; C. G. Pierpont, *Coord. Chem. Rev.*, 2001, **219–221**, 415; (*c*) W. Kaim, *Dalton. Trans.*, 2003, 761.

2 J. W. Whittaker, *Chem. Rev.*, 2003, **103**, 2347.

3 (*a*) M. M. Whittaker, P. J. Kersten, N. Nakamura, J. Sanders-Loehr, E. S. Schweizer and J. W. Whittaker, *J. Biol. Chem.*, 1996, **271**, 681; (*b*) M. M. Whittaker, P. J. Kersten, D. Cullen and J. W. Whittaker, *J. Biol. Chem.*, 1999, **274**, 36226.

4 (*a*) J. Stubbe and W. A. van der Donk, *Chem. Rev.*, 1998, **98**, 705; (*b*) J. Stubbe, D. G. Nocera, C. S. Yee and M. C. Y. Chang, *Chem. Rev.*, 2003, **103**, 2167.

5 (*a*) E. R. Altwicker, *Chem. Rev.*, 1967, **67**, 475; (*b*) P. Gütlich and A. Dei, *Angew. Chem., Int. Ed. Engl.*, 1997, **36**, 2734; (*c*) D. A. Shultz in *Magnetoscience—From Molecules to Materials*, ed. S. Miller and M. Drillon, Wiley–VCH, New York, 2001.

6 (*a*) L. Benisvy, A. J. Blake, D. Collison, E. S. Davies, C. D. Garner, E. J. L. McInnes, J. McMaster, G. Whittaker and C. Wilson, *Chem. Commun.*, 2001, 1824; (*b*) L. Benisvy, A. J. Blake, D. Collison, E. S. Davies, C. D. Garner, E. J. L. McInnes, J. McMaster, G. Whittaker and C. Wilson, *Dalton. Trans.*, 2003, 1975; (*c*) L. Benisvy, A. J. Blake, D. Collison, E. S. Davies, C. D. Garner, E. J. L. McInnes, J. McMaster and C. Wilson, *J. Inorg. Biochem*, 2003, **96**, 101.

7 J. Cosier and A. M. Glazer, *J. Appl. Crystallogr.*, 1986, **19**, 105.

8 G. M. Sheldrick, SHELX-86–97, *Acta Crystallogr., Sect. A.*, 1990, **46**, 467.

9 A. Sokolowski, E. Bothe, E. Bill, T. Weyhermüller and K. Wieghardt, *Chem. Commun.*, 1996, 1671.

10 J. D. Crane, E. Sinn and B. Tann, *Polyhedron*, 1999, **18**, 1527 and references therein.

11 (*a*) C. K. Prout, E. E. Castellano, O. J. R. Hodder and P. J. Sadler, *J. Chem. Soc. A*, 1971, 2620; (*b*) E. D. McKenzie, S. J. Selvey and I. W. Nowell, *Inorg. Chim. Acta*, 1985, **101**, 85; (*c*) H. Sakiyama, h. Okawa, M. Hishashi, N. Matsumoto and S. Kida, *Bull. Chem. Soc. Jpn.*, 1991, **64**, 2644.

12 R. H. Holm, G. W. Everett, Jr. and A. Chakravorty, *Prog. Inorg. Chem.*, 1966, **7**, 83 and references therein.

13 (*a*) P. Ganis, A. Saporito, A. Vitagliano and G. Valle, *Inorg. Chim. Acta*, 1988, **142**, 75; (*b*) M. Winter, J. Sander and K. Hegetschweiler, *Z. Krist.-New Cryst. Struct.*, 2001, **216**, 108.

14 L. Benisvy, G. McArdle, E. S. Davies, C. D. Garner, J. McMaster and C. Wilson, in preparation.

15 J. Müller, A. Kikuchi, E. Bill, T. Weyhermüller, P. Hildebrandt, L. Ould-Moussa and K. Wieghardt, *Inorg. Chim. Acta.*, 2000, **297**, 265.

16 A. Sokolowski, B. Adam, T. Weyhermüller, A. Kikuchi, K. Hildenbrand, R. Schnepf, P. Hildebrandt, E. Bill and K. Wieghardt, *Inorg. Chem.*, 1997, **36**, 3702.

17 F. N. Penkert, T. Weyhermüller, E. Bill, P. Hildebrandt, S. Lecomte and K. Wieghardt, *J. Am. Chem. Soc.*, 2000, **122**, 9663.

18 S. Kimura, E. Bill, E. Bothe, T. Weyhermüller and K. Wieghardt, *J. Am. Chem. Soc.*, 2001, **123**, 6025.